

STANDARD SANC MODULES FOR NLO QCD RADIATIVE CORRECTIONS TO SINGLE TOP-QUARK PRODUCTION

D. Bardin^{a,1}, *S. Bondarenko*^{a,2}, *P. Christova*^{a,3}, *L. Kalinovskaya*^{a,b,4},
V. Kolesnikov^{a,5}, *V. von Schlippe*^{c,6}, *K. Yordanova*^{d,7}

^a Joint Institute for Nuclear Research, Dubna

^b Higher Mathematics Department, the «Dubna» International University for Nature, Society,
and Man, Dubna, Russia

^c B. P. Konstantinov Petersburg Nuclear Physics Institute, RAS, St. Petersburg, Russia

^d Bishop Konstantin Preslavsky University, Shoumen, Bulgaria

In this paper we present the results obtained with the newly created standard SANC modules for calculation of the NLO QCD corrections to single top-quark-production processes in s and t channels at the partonic level, as well as to top-decays. The main aim of these results is to prove the correct work of modules. A comprehensive comparison with the results of the CompHEP system is given, where possible. These modules are intended to be used in Monte Carlo generators for single top-quark-production processes at the LHC. As in our recent paper, devoted to the electroweak corrections to these processes, we study the regularization of the top-legs associated infrared divergences with the aid of the complex mass of the top quark. A comparison of QCD corrections with those computed by the conventional method is presented both for top production and for decays. For s -channel production we give an analytic proof of equivalence of the two methods in the limit of low top width.

Представлены результаты, полученные с помощью новых стандартных SANC модулей для вычисления NLO КХД-поправок к процессам одиночного рождения топ-кварка в s - и t -каналах на партонном уровне, а также для топ-распадов. Основное назначение этих результатов — подтвердить правильность работы модулей. Представлено обширное сравнение результатов с результатами системы CompHEP, где это возможно. Предполагается, что эти модули найдут применение в генераторах Монте-Карло для процессов одиночного рождения топ-кварка на LHC. Как и в нашей последней работе, посвященной электрослабым поправкам к этим процессам, мы исследовали регуляризацию инфракрасной расходимости, связанной с излучением из топ-кварка, с помощью комплексной массы топ-кварка. Также показано сравнение результатов для КХД-поправок, полученных этим методом, с результатами стандартного вычисления для процессов рождения и распадов. Для s -канала рождения аналитически показана эквивалентность двух методов в пределе малой ширины топ-кварка.

PACS: 12.15.Lk; 13.40.Ks; 14.65.Ha; 12.38.-t

¹E-mail: bardin@numail.jinr.ru

²E-mail: bondarenko@jinr.ru

³E-mail: penchris@numail.jinr.ru

⁴E-mail: kalinov@numail.jinr.ru

⁵E-mail: kolesnik@numail.jinr.ru

⁶E-mail: schlippe@thd.pnpi.spb.ru

⁷E-mail: kyspasova@yahoo.co.uk

INTRODUCTION

There is continued interest in precision calculations of single top-quark-production cross sections for the Tevatron and LHC (see, e.g., [1] and references therein). This is motivated to a large extent by the fact that this process is the only way of measuring the CKM matrix element $|V_{tb}|$ directly, providing a sensitive test of the 3-generation scheme of the Standard Model, and that it is an important background to various processes beyond the SM, including Higgs-boson production.

Moreover, such events are already observed at the Tevatron experiments D0 [2,3] and CDF [4,5] and at the LHC [6]. There is a need to prepare software for precision analysis of the high statistics samples of single top-quark events in future measurements at the LHC, running at 7 and 14 TeV.

Most of the theoretical work on single top-quark production has been concerned with NLO QCD corrections (see, e.g., [7,8]), leading to the development of Monte Carlo generators, such as ZTOP [9], MC@NLO [10] or SingleTop [11], incorporated in the standard LHC tools.

In our previous paper [12] we have presented the calculation of the cross sections with one-loop electroweak corrections, regulating the infrared divergences (IRD) associated with the top-quark leg by introducing the width of the top quark.

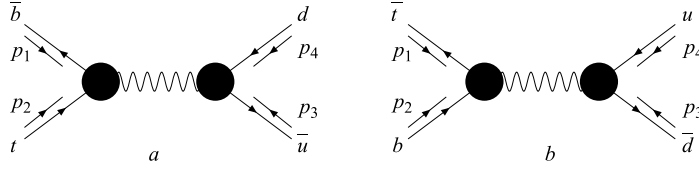
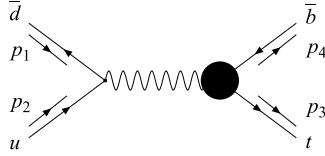
In the present paper we extend that approach to the calculation of one-loop QCD corrections in the spirit of the complex-mass scheme [13]. To our knowledge, there is no other work utilizing this approach to the IRD regularization among the many papers dealing with higher order QCD corrections to single top-quark production, see, e.g., [14] and references therein, as well as papers devoted to the complex-mass scheme itself, e.g., [15,16].

This paper should be read together with [12], whose structure we have taken over here. In Sec. 1 we recall the covariant amplitude for all processes $t\bar{b}u\bar{d} \rightarrow 0$ and $\bar{t}bu\bar{d} \rightarrow 0$ and show the conversions to the processes of t and \bar{t} decay and to s - and t -channel single top-quark production, and point out the essential differences between the EW and QCD formulations of these processes. In Sec. 2 we discuss in detail the regularization of single t - and \bar{t} -quark production in the conventional approach — with zero top-quark width — and in the complex top-quark mass approach. We present explicit formulas derived for both the cases. In Sec. 3 we present the results of numerical calculations which show the stability against variations of the soft-hard separation parameter and of the top-quark width. Finally, in Sec. 4 we present our conclusions and outlook to further work on single top-quark production within the framework of SANC, aimed at the creation of an MC generator that simultaneously takes account of NLO EW and QCD corrections in the so-called 5F-scheme [8].

1. COVARIANT AMPLITUDE

In this section we proceed in the spirit of the «multichannel approach» developed in [17] and [18], and follow closely the presentation of our previous paper [12]. First, we consider annihilation into vacuum with all particles incoming.

1.1. All Particles Incoming. In QCD, there is no contribution from box diagrams such as those of [12] Figs. 1, 2 which were appropriate for the EW case. Therefore in the present case we have a sum of two one-loop vertices instead of the two vacuum diagrams of [12]. The Covariant Amplitudes (CA) of Fig. 1 are characterized by four different structures and scalar

Fig. 1. The $t\bar{b}u\bar{d} \rightarrow 0$ and $t\bar{b}u\bar{d} \rightarrow 0$ processesFig. 2. The FSR in the $\bar{d}u \rightarrow \bar{t}b(g)$ processes

Form Factors (FF) if the masses of the light quarks but not the b -quark mass are neglected. A common expression for this CA in terms of four scalar form factors, $\mathcal{F}_{LL,RL,LD,RD}(s,t)$, was presented in [17]. We recall it here to introduce the notation:

$$\mathcal{A} = i e^2 \frac{d_W(s)}{4} [\gamma_\mu \gamma_+ \otimes \gamma_\mu \gamma_+ \mathcal{F}_{LL}(s,t) + \gamma_\mu \gamma_- \otimes \gamma_\mu \gamma_+ \mathcal{F}_{RL}(s,t) + \\ + \gamma_+ \otimes \gamma_\mu \gamma_+ (-iD_\mu) \mathcal{F}_{LD}(s,t) + \gamma_- \otimes \gamma_\mu \gamma_+ (-iD_\mu) \mathcal{F}_{RD}(s,t)],$$

where

$$\gamma_\pm = (1 \pm \gamma_5), \quad D_\mu = (p_1 - p_2)_\mu.$$

Four-momentum conservation reads

$$p_1 + p_2 + p_3 + p_4 = 0,$$

and the invariants are defined by

$$s = -(p_1 + p_2)^2, \quad t = -(p_2 + p_3)^2, \quad u = -(p_1 + p_3)^2,$$

with

$$s + t + u = m_t^2 + m_b^2.$$

Furthermore,

$$d_W(s) = \frac{V}{2s_w^2} \frac{1}{s - M_W^2 + iM_W\Gamma_W},$$

where $V = V_{tb}V_{ud}$ is the relevant product of CKM matrix elements. The scalar form factors \mathcal{F} are labeled according to their structures, see [17].

1.2. Conversion to Top Decay. The CA for the decay $t(p_2) \rightarrow b(p_1) + u(p_3) + \bar{d}(p_4)$ is derived from Fig. 1, *a* by the following 4-momentum replacement:

$$p_1 \rightarrow -p_1, \quad p_3 \rightarrow -p_3, \\ p_2 \rightarrow p_2, \quad p_4 \rightarrow -p_4.$$

For the decay $\bar{t}(p_1) \rightarrow \bar{b}(p_2) + d(p_3) + \bar{u}(p_4)$ it is more transparent to make the replacement from Fig. 1, *b*:

$$\begin{aligned} p_1 &\rightarrow p_1, & p_3 &\rightarrow -p_3, \\ p_2 &\rightarrow -p_2, & p_4 &\rightarrow -p_4. \end{aligned}$$

The corresponding two physical subprocess diagrams are those shown in Figs. 3, 4 of [12].

1.3. Conversion to *s* Channel. The CA for the *s* channel single top-quark-production processes $\bar{u}(p_1) + d(p_2) \rightarrow b(p_3) + \bar{t}(p_4)$ is obtained from Fig. 1, *a* by the replacement:

$$\begin{aligned} p_1 &\rightarrow -p_3, & p_3 &\rightarrow p_1, \\ p_2 &\rightarrow -p_4, & p_4 &\rightarrow p_2, \end{aligned}$$

and for the processes $\bar{d}(p_1) + u(p_2) \rightarrow t(p_3) + \bar{b}(p_4)$ from Fig. 1, *b* by the conversion:

$$\begin{aligned} p_1 &\rightarrow -p_3, & p_3 &\rightarrow p_1, \\ p_2 &\rightarrow -p_4, & p_4 &\rightarrow p_2. \end{aligned}$$

As a result, we get the two physical subprocess diagrams shown in Figs. 5, 6 of [12].

1.4. Conversion to *t*-Channel Processes. In the CAs for the *t*-channel single top-quark-production processes $\bar{b}(p_1) + \bar{u}(p_2) \rightarrow \bar{d}(p_3) + \bar{t}(p_4)$ and $\bar{b}(p_1) + d(p_2) \rightarrow u(p_3) + \bar{t}(p_4)$, it is convenient to make the replacement «in pairs». From Fig. 1, *a* one may perform two 4-momentum replacements:

$$\begin{aligned} p_1 &\rightarrow p_1, & p_1 &\rightarrow p_1, \\ p_2 &\rightarrow -p_4, & p_2 &\rightarrow -p_4, \\ p_3 &\rightarrow p_2, & p_3 &\rightarrow -p_3, \\ p_4 &\rightarrow p_3, & p_4 &\rightarrow p_2, \end{aligned}$$

which give rise to two different physical *t*-channel processes as shown in Fig. 7 of [12].

For the processes $b(p_1) + u(p_2) \rightarrow t(p_4) + d(p_3)$ and $b(p_1) + \bar{d}(p_2) \rightarrow t(p_4) + \bar{u}(p_3)$, the pair of replacements from Fig. 1, *b*,

$$\begin{aligned} p_1 &\rightarrow -p_4, & p_1 &\rightarrow -p_4, \\ p_2 &\rightarrow p_1, & p_2 &\rightarrow p_1, \\ p_3 &\rightarrow -p_3, & p_3 &\rightarrow p_2, \\ p_4 &\rightarrow p_2, & p_4 &\rightarrow -p_3, \end{aligned}$$

gives the corresponding pair of symbolic diagrams for the two remaining *t*-channel processes. They are shown in Fig. 8 of [12].

2. PROCESS $ud \rightarrow tb$ AT NLO QCD

2.1. Notation and Terminology. After conversion of the vacuum annihilation diagrams of Fig. 1 to the *s* channel, we will have two physical annihilation diagrams for both *t* and \bar{t} production (cf. symbolic diagrams in Figs. 5, 6 of [12]). For our purpose it is sufficient to consider the top production NLO diagrams of Fig. 6 which, in turn, consist of ISR and FSR NLO contributions like the two fat vertices in the diagrams in Fig. 1, standing for emission (and reabsorption) of a real (or virtual) gluon (cf. diagrams in Figs. 9, 10, and 12 of [12]).

Since we are interested in the effects of the top-quark width, the subject of our study will be only the symbolic FSR NLO diagram of Fig. 2. In the following, the label FSR will be assumed and omitted. It should be emphasized also that all the formulae of this section refer to the limit $m_b \rightarrow 0$. We will use the following common terminology:

- LO (or Born);
- NLO = Virtual + Real;
- Real = Soft + Hard;
- SV = Soft + Virtual (with $2 \rightarrow 2$ phase space);
- NLO = SV+HA (Hard Bremsstrahlung with $2 \rightarrow 3$ phase space).

2.2. Conventional Approach. In the conventional approach (stable particles) one introduces a soft–hard separation parameter

$$\bar{\omega} = 1 - \frac{s'_{\max}}{s}, \quad E_g^{\min} = \frac{\sqrt{s}}{2}\bar{\omega},$$

with invariants $s = M_{a,b}^2$ and $s' = M_{c,d}^2$ for the radiative processes $a + b \rightarrow c + d + g$.

And for the total NLO cross sections we have

$$\sigma^{\text{NLO}}(s) = \sigma^{\text{SV}}(s, \bar{\omega}) + \sigma^{\text{HA}}(s, \bar{\omega}).$$

The infrared divergence cancels inside $\sigma^{\text{SV}} = \sigma^{\text{S+V}}$ no matter how it is regularized (dimensionally or by a fictitious photon mass λ), while the $\bar{\omega}$ divergence cancels in the sum $\sigma^{\text{NLO}} = \sigma^{\text{SV+HA}}$, so that σ^{NLO} is finite.

At the end of this paragraph, we list the individual contributions.

Soft + Virtual:

$$\begin{aligned} \sigma^{\text{SV}}(s, \bar{\omega}) = k_0 \left\{ \sigma^{\text{Born}}(s) \left[-2 + (L_s - 2) \ln(\bar{\omega}) + \left(\frac{3}{4} - L_{t1} \right) L_b + \right. \right. \\ \left. \left. + \left(\frac{3}{2} \frac{m_t^2}{s_t} + \frac{5}{2} - 2L_{t1} \right) L_{t1} + \left(\frac{5}{2} \frac{m_t^2}{s_t} + \frac{3}{4} - 2L_{t1} \right) L_t + 2\text{Li}_2 \left(\frac{m_t^2}{s} \right) + 2\text{Li}_2(1) \right] - \right. \\ \left. - \frac{9}{4} K m_t^2 \frac{s_t}{s} (L_{t1} + L_t) \right\}. \quad (1) \end{aligned}$$

Hard:

$$\begin{aligned} \sigma^{\text{HA}}(s, \bar{\omega}) = k_0 \left\{ \sigma^{\text{Born}}(s) \left[\frac{9}{4} - \frac{m_t^2}{s_t} - (L_s - 2) \ln(\bar{\omega}) - \left(\frac{3}{4} - L_{t1} \right) L_b - \right. \right. \\ \left. \left. - \left(\frac{7}{2} - 2L_{t1} \right) L_{t1} - \left(\frac{3}{4} - L_{t1} \right) L_t - 2\text{Li}_2(1) \right] + \frac{1}{2} K (s_t + 2m_t^2 L_t) \right\}. \quad (2) \end{aligned}$$

Born or LO:

$$\sigma^{\text{Born}}(s) = \frac{1}{2} K \frac{s_t^2}{s^2} (2s + m_t^2).$$

Here and below:

$$k_0 = \frac{\alpha_s C_f}{\pi}, \quad K = \frac{G_F^2 M_W^4 V^2}{6\pi[(s - M_W^2)^2 + M_W^2 \Gamma_W^2]},$$

$$L_s = 2 \ln \left(\frac{s_t}{m_t m_b} \right), \quad L_t = \ln \left(\frac{s}{m_t^2} \right), \quad L_b = \ln \left(\frac{s}{m_b^2} \right),$$

$$L_{t1} = \ln \left(1 - \frac{m_t^2}{s} \right), \quad s_t = s - m_t^2.$$

In the NLO cross section all divergences, including b -mass collinear divergences, cancel. The final expression is finite and very compact:

$$\sigma^{\text{NLO}}(s) = k_0 \left\{ \sigma^{\text{Born}}(s) \left[\frac{3}{4} - (L_t + 1)L_{t1} + 2\text{Li}_2 \left(\frac{m_t^2}{s} \right) \right] + \frac{1}{4} K \frac{m_t^2}{s^2} \left[(5s_t(s + m_t^2) + 4m_t^2 s)L_t - 3s_t^2(L_{t1} + 1) - 4m_t^2 s_t \right] \right\}. \quad (3)$$

2.3. Infrared Regularization by the Complex Top-Quark Mass. The main aim of this paragraph is to show that the infrared regularization by the complex top-quark mass leads exactly to the same final result, Eq.(3), though the partial expressions for SV and HA have a completely different form. For the introduction to the problem, we refer the reader to Sec.3 of [12]. Here we again only list the individual contributions to the total cross sections.

Soft + Virtual:

$$\sigma^{\text{SV}}(s, \bar{\omega}, \Gamma_t) = k_0 \left\{ \sigma^{\text{Born}}(s) \left[-1 - (1 - L_s) \ln \left(\frac{\Gamma_t}{m_t} \right) - \ln(\bar{\omega}) + \left(\frac{3}{4} - L_{t1} - L_t \right) L_b + \left(\frac{3}{4} - 3L_{t1} - \frac{1}{2}L_t \right) L_t + \left(\frac{5}{2} - 2L_{t1} \right) L_{t1} + \text{Li}_2 \left(\frac{m_t^2}{s} \right) + 3\text{Li}_2(1) \right] - \frac{3}{4} K m_t^2 \frac{s_t^2}{s^2} (L_{t1} + L_t) \right\}. \quad (4)$$

Hard:

$$\sigma^{\text{HA}}(s, \bar{\omega}, \Gamma_t) = k_0 \left\{ \sigma^{\text{Born}}(s) \left[\frac{5}{4} - \frac{m_t^2}{s_t} + (1 - L_s) \ln \left(\frac{\Gamma_t}{m_t} \right) + \ln(\bar{\omega}) - \left(\frac{3}{4} - L_{t1} - L_t \right) L_b - \left(\frac{7}{2} - 2L_{t1} \right) L_{t1} - \left(\frac{3}{4} - \frac{m_t^2}{s_t} - 2L_{t1} - \frac{1}{2}L_t \right) L_t + \text{Li}_2 \left(\frac{m_t^2}{s} \right) - 3\text{Li}_2(1) \right] + \frac{1}{2} K (s_t + 2m_t^2 L_t) \right\}. \quad (5)$$

We note the presence of two regularization parameters: $\bar{\omega}$ is due to conventional treatment of infrared divergences associated with b -quark legs, and $\ln(\Gamma_t/m_t)$ is a new regularization parameter associated with the t -quark leg, whose infrared divergence is regularized by its width. The individual (SV and HA contributions) have completely different form, but they sum up to exactly the same finite NLO expression (3) in which all three types of divergent terms ($\ln(\Gamma_t/m_t)$, $\ln(\bar{\omega})$, $\ln(m_b)$) have canceled.

2.4. Relevant AV Functions. The virtual contributions (due to vertex, Fig. 10, and the counter-term, Fig. 9, of [12]) were computed using the standard Passarino–Veltman reduction [19]. The relevant C_0 function

$$C_0(-m_t^2, -m_b^2, Q^2; \tilde{m}_t, 0, m_b),$$

with complex argument

$$\tilde{m}_t^2 = m_t^2 + \Delta_t, \quad \Delta_t = -im_t\Gamma_t,$$

is given by Eqs.(22)–(24) of [12] and its limit at $m_b \rightarrow 0$ by Eqs.(25), (26) of that paper. Below we present its real part double limit: $m_b \rightarrow 0$ and $\Gamma_t \rightarrow 0$, which was used in the derivation of Eq. (4):

$$\begin{aligned} \text{Re } C_0(-m_t^2, -m_b^2, -s; \tilde{m}_t, 0, m_b) = & \frac{1}{s_t} \left\{ \left[\ln \left(\frac{\Gamma_t}{m_t} \right) - L_{t1} - L_t \right] (L_b + L_t + 2L_{t1}) + \right. \\ & \left. + L_{t1}L_t + \frac{1}{2}L_t^2 - \text{Li}_2 \left(1 - \frac{m_t^2}{s} \right) + 4\text{Li}_2(1) \right\}. \end{aligned}$$

In the calculation of the counter-term, one meets the real part of the derivative of a B_0 function:

$$\text{Re } [B'_0(-m_t^2, 0, \tilde{m}_t)] = \frac{1}{m_t^2} \ln \left(\frac{\Gamma_t}{m_t} \right).$$

2.5. Differential in s' Hard-Gluon Radiation. The hard-gluon contributions, Eqs.(2) and (5), were derived by 4-fold integration in the $2 \rightarrow 3$ process phase space over three angular variables and over the invariant s' , which varies within the limits $m_t^2 \leq s' \leq s'_{\text{max}}$. In this paragraph we present the s' integrands for the two approaches under consideration.

2.5.1. Conventional Approach. In the conventional approach, the expression for $\sigma^{\text{HA}}(s, s')$ is well known:

$$\sigma^{\text{HA}}(s, s') = k_0 \left\{ \sigma^{\text{Born}}(s)(2 - L_{s'}) \left(\frac{1}{s_t} - \frac{1}{s - s'} \right) - K \frac{s - s'}{s} \left(\frac{s'_t}{s'} - k_1 L_{s'} \right) \right\},$$

where

$$k_1 = \frac{1}{2} \left(1 + \frac{1}{2} \frac{m_t^2}{s} \right), \quad L_{s'} = 2 \ln \left(\frac{s'_t}{m_t m_b} \right), \quad s'_t = s' - m_t^2.$$

The $\bar{\omega}$ divergent term $1/(s - s')$ after integration over s' gives rise to $\ln(\bar{\omega})$ terms in Eq. (2) which cancel the corresponding terms in Eq. (1).

2.5.2. Infrared Regularization by the Complex Top-Quark Mass. The expression for $\sigma^{\text{HA}}(s, s')$ is more complicated in this case:

$$\begin{aligned} \sigma^{\text{HA}}(s, s') = k_0 \left\{ \sigma^{\text{Born}}(s) \left[\frac{1}{s_t} - \frac{1}{s - s'} + \frac{k^+}{2} L'_{s'} - \frac{1}{s_t} L_{s'} - \right. \right. \\ \left. \left. - \frac{1}{2} (I_1(s') + I_2(s')) - \frac{m_t^2}{s_t} I_3(s') \right] - K \frac{s - s'}{s} \left(\frac{s'_t}{s'} - k_1 L_{s'} \right) \right\}. \quad (6) \end{aligned}$$

Here,

$$L'_{s'} = L_{s'} - \ln\left(\frac{s'}{m_b^2}\right),$$

$$k^\pm = \frac{1}{s - s' + i\gamma_t} \pm \frac{1}{s - s' - i\gamma_t},$$

$$\gamma_t = \Gamma_t m_t.$$

The three nontrivial objects to be integrated are:

$$I_1(s') = k^+ \operatorname{Re}(J_b^W(0, m_t, \sqrt{s'}, i\gamma_t)),$$

$$I_2(s') = ik^- \operatorname{Im}(J_b^W(0, m_t, \sqrt{s'}, i\gamma_t)),$$

$$I_3(s') = \frac{1}{\gamma_t} \operatorname{Im}(J_b^W(0, m_t, \sqrt{s'}, i\gamma_t)),$$

where

$$J_b^W(0, m_t, \sqrt{s'}, i\gamma_t) = \ln\left(\frac{i\gamma_t s' + (s - s')m_t^2}{i\gamma_t s' + (s - s')s'}\right),$$

and «0» in the argument list stands for the limit $m_b \rightarrow 0$.

Taking the integrals

$$I_i(s) = \int_{m_t^2}^s I_i(s') ds', \quad i = 1, 2, 3,$$

we get

$$I_1(s) = \ln\left(\frac{s}{m_t^2}\right) \left[\ln\left(\frac{\Gamma_t^2}{m_t^2}\right) - 2 \ln\left(\frac{s_t}{m_t^2}\right) \right] -$$

$$- \operatorname{Li}_2\left(\frac{-s_t}{m_t^2}\right) + 2 \operatorname{Li}_2\left(\frac{s_t}{s}\right) - \operatorname{Li}_2\left(1 + \frac{s}{m_t^2}\right) + \frac{3}{2} \operatorname{Li}_2(1), \quad (7)$$

$$I_2(s) = -\operatorname{Li}_2\left(\frac{-s_t}{m_t^2}\right) + \operatorname{Li}_2\left(1 + \frac{s}{m_t^2}\right) - \frac{3}{2} \operatorname{Li}_2(1),$$

$$I_3(s) = \frac{1}{m_t^2} \left[-s_t \ln\left(\frac{\Gamma_t}{m_t}\right) + s_t \ln\left(\frac{-s_t}{m_t^2}\right) - m_t^2 \ln\left(\frac{s}{m_t^2}\right) \right].$$

Substituting Eqs. (7) into Eq. (6) we arrive at Eq. (5).

3. NUMERICAL RESULTS

In this section we present the SANC results for the cross sections of the single top-quark-production processes and for the top-quark decays. The tree level contributions, both Born and single real gluon emission, are compared with CompHEP v.4.4.3 [20] and v.4.5.1 [21]. All numerical results for this section were produced with the standard SANC INPUT working in the $\alpha(0)$ EW scheme.

The SANC input parameters set:

$$\begin{aligned}
G_F &= 1.16637 \cdot 10^{-5} \text{ GeV}^{-2}, & \alpha_s &= 0.107, \\
\alpha(0) &= 1/137.035999, & \Gamma_W &= 2.141 \text{ GeV}, \\
M_W &= 80.403 \text{ GeV}, & \Gamma_Z &= 2.4952 \text{ GeV}, \\
M_Z &= 91.1876 \text{ GeV}, & \Gamma_t &= 1.5517 \text{ GeV}, \\
M_H &= 120 \text{ GeV}, & m_d &= 83 \text{ MeV}, \\
m_u &= 62 \text{ MeV}, & m_s &= 215 \text{ MeV}, \\
m_c &= 1.5 \text{ GeV}, & m_b &= 4.7 \text{ GeV}, \\
m_t &= 174.2 \text{ GeV}, & & \\
|V_{ud}| &= 1, & |V_{cs}| &= 1, \\
|V_{us}| &= 0, & |V_{cd}| &= 0. \\
|V_{tb}| &= 1. & &
\end{aligned} \tag{8}$$

Numbers used for the comparison with CompHEP for the decay channels were produced with CompHEP v.4.4.3 and with v.4.5.1 for the production channels. For this comparison we use the standard CompHEP setup and the $\alpha(0)$ EW scheme, however, we used $\alpha_s = 0.12201(Q = M_Z)$ and $m_u = m_d = 66$ MeV. Moreover, in both codes we use the «fixed t -width scheme».

The structure, notation and terminology used of this section are very similar to those of the corresponding Sec. 4 of [12]. We refer the reader to the paragraphs that follow Eq. (33) and do not repeat here Eqs. (34), (35) and the surrounding text of the latter paper.

3.1. Decay Channels $t \rightarrow b + u + \bar{d}$. *3.1.1. SANC–CompHEP Comparison.* In Table 1 we present results of the SANC–CompHEP comparison of radiative decay width Γ^{hard} in MeV for two cuts on the gluon energy: $E_g \geq 5, 10$ GeV (in the top rest frame) and for two options: $\Gamma_t = 0(\neq 0)$ and six channels pid = 19–24 for the case of SANC (pid = 19, 21, 23 for \bar{t} decays, pid = 20, 22, 24 for t decays).

Table 1. SANC–CompHEP comparison of decay width Γ^{hard} in MeV in the α scheme for two options: $\Gamma_t = 0(\neq 0)$; and for six channels pid = 19–24

Program, pid	$E_g = 5$ GeV		$E_g = 10$ GeV	
	$\Gamma_t = 0$	$\Gamma_t \neq 0$	$\Gamma_t = 0$	$\Gamma_t \neq 0$
$t \rightarrow b + e^+ + \bar{\nu}_e + g$				
CompHEP	72.29(1)	71.80(2)	47.24(2)	47.13(2)
SANC, pid = 19	72.28(1)	71.79(1)	47.20(1)	47.10(1)
SANC, pid = 20	72.28(1)	71.79(1)	47.20(1)	47.10(1)
$t \rightarrow b + \mu^+ + \bar{\nu}_\mu + g$				
CompHEP	72.29(2)	71.80(2)	47.24(2)	47.13(2)
SANC, pid = 21	72.28(1)	71.79(1)	47.20(1)	47.10(1)
SANC, pid = 22	72.28(1)	71.79(1)	47.20(1)	47.10(1)
$t \rightarrow b + u + \bar{d} + g$				
CompHEP	1296.9(6)	1295.6(5)	820.3(3)	819.7(3)
SANC, pid = 23	1296.3(1)	1294.9(1)	819.8(1)	819.5(1)
SANC, pid = 24	1296.3(1)	1294.9(1)	819.8(1)	819.5(1)

The main aim of Table 1 is to demonstrate, for the first time, that there is good agreement between SANC and CompHEP not only for $\Gamma_t = 0$, but also for the $\Gamma_t \neq 0$ options ($\Gamma_t \neq 0$ always refers to the value in Eq. (8)).

3.1.2. An Internal SANC Comparison. In SANC there are two modules for the computation of hard gluon bremsstrahlung processes: fully differential (5D), to be used in Monte Carlo simulations, and two-dimensional ($2s'$) in invariant variables $s = -(p_t - p_b)^2$ and $s' = -(p_u + p_d)^2$, being analytically integrated over all angular variables. In order to check numerically the correctness of the analytic angular integration, we present Table 2 which shows the self-consistency of SANC calculations of the radiative contribution. Note that here E_g is the cut in the s' compound rest frame: this is why the numbers in Tables 1 and 2 are different.

Table 2. SANC comparison of decay width Γ^{hard} in MeV in the $\alpha(0)$ scheme for two options: $\Gamma_t = 0(\neq 0)$; two variants: 5D and $2s'$; and for two channels pid = 22 and 24

Program, pid	$E_g = 5 \text{ GeV}$		$E_g = 10 \text{ GeV}$	
	$\Gamma_t = 0$	$\Gamma_t \neq 0$	$\Gamma_t = 0$	$\Gamma_t \neq 0$
$t \rightarrow b + \mu^+ + \bar{\nu}_\mu + g$				
SANC-5D, pid = 22	96.446(1)	94.459(1)	67.492(1)	67.085(1)
SANC- $2s'$, pid = 22	96.446(1)	94.459(1)	67.493(1)	67.085(1)
$t \rightarrow b + u + \bar{d} + g$				
SANC-5D, pid = 24	1245.6(1)	1239.6(1)	763.09(1)	761.87(1)
SANC- $2s'$, pid = 24	1245.6(1)	1239.6(1)	763.11(1)	761.88(1)

3.1.3. One-Loop Decay Width. The numbers of this section are produced with SANC setup (8) in the $\alpha(0)$ EW parameterization scheme. We present results for two processes: pid = 22 and 24.

- pid = 22. Process $t \rightarrow b + \mu^+ + \bar{\nu}_\mu$.

In Table 3 we show the lowest-order width Γ^{Born} as a function of the b -quark mass. As is seen, the effect of a finite b -quark mass is tiny. This justifies considering the limit $m_b \rightarrow 0$, in which the formulas are much shorter and which is convenient to study the validity of the KLN theorem in NLO approximation.

Table 4 demonstrates the stability of one-loop corrected quantities to the variation of the soft-hard separation parameter E_g .

As is seen from Table 4, there is good E_g stability for $E_g \leq 10^{-1} \text{ GeV}$. However, there is a rather big difference of the results for the one-loop corrected width $\Gamma^{1\text{-loop}}$ and the relative QCD correction δ of the partial decay width between the calculation with the $\Gamma_t = 0$ and the $\Gamma_t \neq 0$ options, where in the latter case we use the fixed₁ scheme defined in [12]. This difference gets smaller with formally decreasing Γ_t , as Table 5 illustrates.

Table 5 demonstrates the two-dimensional convergence of $\Gamma^{1\text{-loop}}$ and δ when both m_b and Γ_t go to zero. Note that with decreasing Γ_t the convergence in m_b improves.

Table 3. The total lowest-order width Γ^{Born} in GeV as a function of m_b

$m_b, \text{ GeV}$	$\Gamma^{\text{Born}}, \text{ GeV}$
4.7	0.149094(1)
1.0	0.149466(1)
0.1	0.149483(1)

Table 4. **The total one-loop corrected width $\Gamma^{1\text{-loop}}$ in GeV and relative one-loop correction $\delta = (\Gamma^{1\text{-loop}} - \Gamma^{\text{Born}})/\Gamma^{1\text{-loop}}$ for $E_g = 10^{-1}, 10^{-2}, 10^{-3}$ GeV and $m_b = 4.7$ GeV**

Width, correction	$E_g = 10^{-1}$ GeV	$E_g = 10^{-2}$ GeV	$E_g = 10^{-3}$ GeV
$\Gamma_t = 0$			
$\Gamma^{1\text{-loop}}$	0.13651(1)	0.13652(1)	0.13651(1)
$\delta, \%$	-8.440(1)	-8.437(2)	-8.439(9)
$\Gamma_t \neq 0$			
$\Gamma^{1\text{-loop}}$	0.13735(1)	0.13734(1)	0.13735(1)
$\delta, \%$	-7.880(2)	-7.883(2)	-7.877(8)

Table 5. **The total one-loop corrected width $\Gamma^{1\text{-loop}}$ in GeV and corresponding relative one-loop correction δ in % as a function of the b -quark mass and of Γ_t with soft-hard separation parameter $E_g = 10^{-2}$ GeV**

$m_b, \text{ GeV}$	$\Gamma_t/10^0$	$\Gamma_t/10^1$	$\Gamma_t/10^2$	$\Gamma_t = 0$
$\Gamma^{1\text{-loop}}, \text{ GeV}$				
4.7	0.137345(2)	0.136594(2)	0.136518(3)	0.136515(3)
1.0	0.137919(2)	0.136840(2)	0.136726(3)	0.136717(3)
0.1	0.138479(2)	0.136900(2)	0.136738(3)	0.136723(5)
$\delta, \%$				
4.7	-7.881(1)	-8.384(1)	-8.436(2)	-8.437(2)
1.0	-7.726(1)	-8.448(1)	-8.523(2)	-8.530(2)
0.1	-7.362(1)	-8.418(1)	-8.526(2)	-8.537(3)

Table 6. **The total lowest-order width Γ^{Born} in GeV as a function of m_b**

$m_b, \text{ GeV}$	$\Gamma^{\text{Born}}, \text{ GeV}$
4.7	0.447284(1)
1.0	0.448399(1)
0.1	0.448451(1)

- pid = 24. Process $t \rightarrow b + u + \bar{d}$.

Here we present the corresponding set of Tables for the quark-decay mode of the top quark.

The total lowest-order width (Table 6) also shows weak sensitivity to variations of the b -quark mass.

The stability against variation of E_g is shown in Table 7.

Similar conclusions as drawn after Table 4 are valid in this case. Finally, Table 8, showing the two-dimensional limit, demonstrates similar behavior as Table 5 for the semileptonic top decay.

3.2. s Channel. Here we consider s -channel processes:

- pid = 25, $\bar{d} + u \rightarrow \bar{b} + t$ and pid = 26, $\bar{u} + d \rightarrow \bar{t} + b$,

but it is sufficient to consider one channel, say pid = 25.

3.2.1. *SANC-CompHEP Comparison.* As is seen from Table 9, there is very good agreement of numbers obtained from SANC and CompHEP within the statistical errors for two considered width options and three cms energies. In this case, the two widths options agree well for all three energies.

3.2.2. *One-Loop Corrections.* The analogue of Tables 4–9 of [12] is now represented by one joint Table 10 showing the stability of one-loop corrected QCD cross sections $\hat{\sigma}^{1\text{-loop}}$ and relative QCD RC δ against variation of the soft-hard separation parameter, $\bar{\omega}$, and the difference between the two options: $\Gamma_t = 0 (\neq 0)$. As is seen, there is good $\bar{\omega}$ stability in the interval $\bar{\omega} = 10^{-5} - 10^{-6}$; also, the subtracted quantities $\hat{\sigma}^{\overline{\text{MS}}}$ and $\delta^{\overline{\text{MS}}}$ for all three cms

Table 7. The total one-loop corrected width $\Gamma^{1\text{-loop}}$ in GeV and relative one-loop correction δ in % for $E_g = 10^{-1}, 10^{-2}, 10^{-3}$ GeV and $m_b = 4.7$ GeV

Width, correction	$E_g = 10^{-1}$ GeV	$E_g = 10^{-2}$ GeV	$E_g = 10^{-3}$ GeV
$\Gamma_t = 0$			
$\Gamma^{1\text{-loop}}$	0.3594(1)	0.3581(1)	0.3584(4)
$\delta, \%$	-19.65(1)	-19.94(1)	-19.89(6)
$\Gamma_t \neq 0, \text{fixed}_1$			
$\Gamma^{1\text{-loop}}$	0.3619(1)	0.3606(1)	0.3607(3)
$\delta, \%$	-19.10(1)	-19.37(1)	-19.35(7)

Table 8. The total one-loop corrected width $\Gamma^{1\text{-loop}}$ in GeV and corresponding relative one-loop correction δ in % for $E_g = 10^{-2}$ GeV as a function of the b -quark mass and of Γ_t

m_b, GeV	$\Gamma_t/10^0$	$\Gamma_t/10^1$	$\Gamma_t/10^2$	$\Gamma_t = 0$
$\Gamma^{1\text{-loop}}, \text{GeV}$				
4.7	0.36054(8)	0.35830(8)	0.35808(8)	0.35812(6)
1.0	0.36210(8)	0.35890(8)	0.35863(8)	0.35870(6)
0.1	0.36380(8)	0.35898(8)	0.35854(8)	0.35861(7)
$\delta, \%$				
4.7	-19.39(2)	-19.89(2)	-19.94(2)	-19.94(1)
1.0	-19.25(2)	-19.96(2)	-20.02(2)	-20.00(1)
0.1	-18.88(2)	-19.95(2)	-20.05(2)	-20.03(2)

Table 9. Comparison of the cross section $\sigma^{\text{hard}}(\sqrt{s}, \Gamma_t)$ in pb for three cms energies and two width options $\Gamma_t = 0(\neq 0)$, for $\text{pid} = 25$, i.e., for process $\bar{d} + u \rightarrow \bar{b} + t$; the E_g cut is equal to 2 GeV

Programme	$\sqrt{s} = 200$ GeV	$\sqrt{s} = 1000$ GeV	$\sqrt{s} = 7000$ GeV
$\Gamma_t = 0$			
CompHEP	0.72930(2)	1.6340(1)	0.071223(1)
SANC-4D	0.72927(1)	1.6341(1)	0.071229(1)
SANC- s'	0.72928(1)	1.6338(1)	0.071227(1)
$\Gamma_t \neq 0$			
CompHEP	0.72638(2)	1.6323(1)	0.070946(1)
SANC-4D	0.72636(1)	1.6322(1)	0.070942(1)
SANC- s'	0.72636(1)	1.6322(1)	0.070942(1)

energies and for both width options, $\Gamma_t = 0(\neq 0)$, are seen to be independent of the light quark masses.

One can see that the difference between the two width options is of order of few per mille in absolute deviation, rapidly decreasing with increasing cms energy. We therefore conclude that one may use the usual infrared regularization for s -channel processes as was the case for EW corrections, see the text after Table 6 of [12].

In Table 11 we demonstrate two-dimensional convergence of $\hat{\sigma}_1^{\overline{\text{MS}}}$ and $\delta^{\overline{\text{MS}}}$ when both m_b and Γ_t go to zero. Note that, similarly to top-decay cases, with lowering of Γ_t the convergence in m_b improves.

Table 10. The total lowest-order cross section σ^{Born} , one-loop cross section $\hat{\sigma}^{\text{1-loop}}$ and total one-loop corrected $\overline{\text{MS}}$ subtracted quantities $\hat{\sigma}^{\overline{\text{MS}}}$ and corresponding δ and $\delta^{\overline{\text{MS}}}$ in % at $\bar{\omega} = 10^{-5}, 10^{-6}$ for $\sqrt{s} = 200, 1000, 7000$ GeV

\sqrt{s} , GeV	200		1000		7000	
σ^{Born} , fb	308.09055(1)		105.97718(1)		2.2352950(1)	
$\bar{\omega}$	10^{-5}	10^{-6}	10^{-5}	10^{-6}	10^{-5}	10^{-6}
$\Gamma_t = 0, m_q$						
$\hat{\sigma}^{\text{1-loop}}$	-374.05(1)	-374.07(1)	0.36446(1)	364.46(1)	17.599(1)	17.599(1)
δ , %	-221.41(1)	-221.42(1)	243.90(1)	243.90(1)	687.34(1)	687.34(1)
$\hat{\sigma}^{\overline{\text{MS}}}$	525.34(1)	525.37(1)	0.17057(1)	170.57(1)	8.2097(1)	8.2097(1)
$\delta^{\overline{\text{MS}}}$, %	70.51(1)	70.53(1)	60.95(1)	60.95(1)	267.28(1)	267.28(1)
$\Gamma_t = 0, m_q/10$						
$\hat{\sigma}^{\overline{\text{MS}}}$	525.34(1)	525.37(1)	0.17057(1)	170.57(1)	8.2097(1)	8.2097(1)
$\delta^{\overline{\text{MS}}}$, %	70.51(1)	70.52(1)	60.95(1)	60.95(1)	267.27(1)	267.28(1)
$\Gamma_t \neq 0, m_q$						
$\sigma^{\text{1-loop}}$	-372.85(1)	-372.87(1)	0.36455(1)	364.55(1)	17.601(1)	17.601(1)
δ , %	-221.02(1)	-221.03(1)	243.99(1)	243.99(1)	687.40(1)	687.40(1)
$\hat{\sigma}^{\overline{\text{MS}}}$	526.54(1)	526.57(1)	0.17066(1)	170.66(1)	8.2111(1)	8.2111(1)
$\delta^{\overline{\text{MS}}}$, %	70.90(1)	70.91(1)	61.03(1)	61.03(1)	267.34(1)	267.34(1)
$\Gamma_t \neq 0, m_q/10$						
$\hat{\sigma}^{\overline{\text{MS}}}$	526.54(1)	526.57(1)	0.17066(1)	170.66(1)	8.2111(1)	8.2111(1)
$\delta^{\overline{\text{MS}}}$, %	70.90(1)	70.91(1)	61.03(1)	61.03(1)	267.34(1)	267.34(1)

Table 11. The total one-loop corrected $\overline{\text{MS}}$ subtracted cross sections $\hat{\sigma}^{\overline{\text{MS}}}$ in pb and corresponding relative one-loop correction $\delta^{\overline{\text{MS}}}$ in % for $\sqrt{\hat{s}} = 200$ GeV (at the parton level) and for $\bar{\omega} = 10^{-5}$ as a function of the b -quark mass and of Γ_t

m_b , GeV	$\Gamma_t/10^0$	$\Gamma_t/10^2$	$\Gamma_t/10^4$	$\Gamma_t = 0$
$\hat{\sigma}^{\overline{\text{MS}}}$, pb				
4.7	0.52654(1)	0.52530(1)	0.52534(1)	0.52534(1)
1.0	0.53099(1)	0.52783(1)	0.52776(1)	0.52778(1)
0.1	0.53386(1)	0.52791(1)	0.52784(1)	0.52784(1)
0.01	0.53656(1)	0.52793(1)	0.52783(1)	0.52785(1)
$\delta^{\overline{\text{MS}}}$, %				
m_b , GeV	$\Gamma_t/10^0$	$\Gamma_t/10^2$	$\Gamma_t/10^4$	$\Gamma_t = 0$
4.7	70.90(1)	70.50(1)	70.52(1)	70.51(1)
1.0	69.65(1)	68.64(1)	68.62(1)	68.62(1)
0.1	70.44(1)	68.54(1)	68.52(1)	68.52(1)
0.01	71.30(1)	68.55(1)	68.52(1)	68.52(1)

The agreement of $\hat{\sigma}_1^{\overline{\text{MS}}}$ and $\delta^{\overline{\text{MS}}}$ in the double limit (numbers for $\Gamma_t/10^4$ and $\Gamma_t = 0$) illustrates our analytic considerations described in Sec. 2.

3.3. t Channel. *3.3.1. SANC–CompHEP Comparison.* This is the most complicated case: t -channel cross sections show up bad statistical convergence. For this comparison we use CompHEP v.4.5.1 and its setup, but with non-zero masses of the u and d quarks (accessed via $bc \rightarrow ts\gamma$ channel). For the Tables of this subsection we used $m_q = m_u = m_d = 66$ MeV and $10m_q$, i.e., $m_u = m_d = 660$ MeV. The cut on the cms gluon energy was $E_g \geq 2$ GeV, and $\alpha_s = 0.12201$ ($Q = M_Z$). As in [12], rows marked «SANC(S)» («S»hort massive case) were computed retaining m_q or $10m_q$ only in fermion propagators radiating a gluon, while «SANC(F)» («F»ully massive case) means that light quark masses were kept everywhere.

- pid = 27: Process $b + u \rightarrow d + t$.
- pid = 28: Process $b + \bar{d} \rightarrow \bar{u} + t$.

The results of Tables 12, 13 are qualitatively the same and may be discussed together.

There is satisfactory agreement for all options only near the reaction threshold. At higher energies SANC/CompHEP agree poorly for the m_q option and much better for the $10m_q$ option. This allows us to draw conclusions similar to those which were drawn at the discussion of the results of analogous Tables 10, 11 of [12].

Table 12. Comparison of the cross section $\hat{\sigma}^{\text{hard}}(\sqrt{s})$ in pb for the process $b + u \rightarrow t + d$ for three cms energies; three options of four: ($\Gamma_t = 0(\neq 0)$) \otimes ($m_q, 10m_q$)

Programme	$\sqrt{s} = 200$	$\sqrt{s} = 1000$	$\sqrt{s} = 7000$
$\Gamma_t = 0, m_q$			
CompHEP	17.908(1)	415.04(6)	617.40(6)
SANC(S)	17.904(1)	416.39(1)	618.94(1)
$\Gamma_t \neq 0, m_q$			
CompHEP	17.761(1)	404.29(6)	574.02(6)
SANC(S)	17.759(1)	405.62(1)	575.61(1)
SANC(F)	17.760(1)	405.63(1)	575.62(1)
$\Gamma_t \neq 0, 10m_q$			
CompHEP	11.792(1)	286.79(7)	400.29(2)
SANC(F)	11.789(1)	287.08(1)	400.48(1)

Table 13. The same as in Table 12, but for the process $b + \bar{d} \rightarrow \bar{u} + t$

Programme	$\sqrt{s} = 200$	$\sqrt{s} = 1000$	$\sqrt{s} = 7000$
$\Gamma_t = 0, m_q$			
CompHEP	10.335(1)	388.74(7)	615.5(1)
SANC(S)	10.332(1)	389.87(1)	616.86(1)
$\Gamma_t \neq 0, m_q$			
CompHEP	10.245(1)	378.21(7)	572.0(1)
SANC(S)	10.241(1)	379.34(1)	573.58(1)
SANC(F)	10.241(1)	379.35(1)	573.59(1)
$\Gamma_t \neq 0, 10m_q$			
CompHEP	6.641(1)	266.75(2)	398.68(4)
SANC(F)	6.640(1)	266.83(1)	398.83(1)

3.3.2. One-Loop QCD Corrections. The numerical results for this subsection were again produced with the aim to demonstrate the stability of one-loop corrected QCD cross sections $\sigma^{1\text{-loop}}$ and relative QCD RC δ against variation of the soft–hard separator $\bar{\omega}$ and to study the difference between the two options: $\Gamma_t = 0 (\neq 0)$.

- pid = 27. Process $b + u \rightarrow d + t$.

Table 14 is the counterpart for QCD of the six Tables 12–17 of [12].

Stability in $\bar{\omega}$ is seen to hold in all considered variants; m_q independence is clearly seen for the $\Gamma_t = 0$ option. However, contrary to EW corrections, the dependence on Γ_t itself for unsubtracted quantities (compare two δ rows) is much more pronounced, varying from several % near the threshold to half a percent at higher energies. Since it is not known how to realize subtraction for $\Gamma_t \neq 0$ option, this difference may be treated as a theoretical uncertainty of NLO calculations which is, however, much smaller than the estimate of NNLO contributions [22].

For t -channel processes, we show only one-dimensional convergence in the limit $\Gamma_t \rightarrow 0$ for $\sqrt{s} = 200$ GeV, where our NLO correction is unphysical ($< -100\%$), see Table 15. (We recall, that in this case we do not have an analytic proof of convergence similar to the

Table 14. The total lowest-order cross section σ^{Born} , one-loop cross section $\hat{\sigma}^{1\text{-loop}}$ and total one-loop corrected $\overline{\text{MS}}$ subtracted quantities $\hat{\sigma}^{\overline{\text{MS}}}$ (all in pb) and corresponding δ and $\delta^{\overline{\text{MS}}}$ in % for $\bar{\omega} = 10^{-5}, 10^{-6}$ and $\sqrt{s} = 200, 1000, 7000$ GeV

\sqrt{s} , GeV	200		1000		7000	
σ^{Born} , pb	7.3551153(1)		48.993407(2)		50.824228(2)	
$\bar{\omega}$	10^{-5}	10^{-6}	10^{-5}	10^{-6}	10^{-5}	10^{-6}
$\Gamma_t = 0, m_q$						
$\hat{\sigma}^{1\text{-loop}}$	−5.741(1)	−5.742(1)	43.67(1)	43.66(1)	50.57(2)	50.57(2)
δ , %	−178.06(1)	−178.07(1)	−10.90(2)	−10.88(3)	−0.50(3)	−0.48(3)
$\hat{\sigma}^{\overline{\text{MS}}}$	10.215(1)	10.215(1)	47.67(1)	47.67(1)	50.71(2)	50.72(2)
$\delta^{\overline{\text{MS}}}$, %	38.88(1)	38.88(1)	−2.70(2)	−2.69(3)	−0.23(3)	−0.20(4)
$\Gamma_t = 0, m_q/10$						
$\hat{\sigma}^{\overline{\text{MS}}}$	10.212(1)	10.210(1)	47.66(2)	47.66(2)	50.71(2)	50.72(3)
$\delta^{\overline{\text{MS}}}$, %	38.88(2)	38.86(2)	−2.73(4)	−2.72(4)	−0.22(5)	−0.21(6)
$\Gamma_t \neq 0, m_q$						
$\sigma^{1\text{-loop}}$	−5.573(1)	−5.574(1)	43.94(1)	43.95(1)	50.87(2)	50.86(2)
δ , %	−175.77(1)	−175.78(1)	−10.29(3)	−10.28(2)	0.097(29)	0.063(34)

Table 15. The total one-loop corrected $\hat{\sigma}^{1\text{-loop}}$ in pb and corresponding δ in % at $\sqrt{s} = 200$ GeV and $\Gamma_t/10^N$, $N = 0, 2, 4$ (the total lowest-order cross section $\sigma^{\text{Born}} = 7.3551153(1)$ pb)

Cross section, correction	$\Gamma_t/10^0$	$\Gamma_t/10^2$	$\Gamma_t/10^4$	$\Gamma_t = 0$
$\hat{\sigma}^{1\text{-loop}}$, pb	−5.5730(6)	−5.7392(6)	−5.7419(7)	−5.7411(6)
δ , %	−175.77(1)	−178.03(1)	−178.07(1)	−178.06(1)

Table 16. The same as in Table 14 but for $\text{pid} = 28$. Process $b + \bar{d} \rightarrow \bar{u} + t$

\sqrt{s} , GeV	200		1000		7000	
σ^{Born} , pb	4.49579065(2)		46.6869560(1)		50.72449(1)	
$\bar{\omega}$	10^{-5}	10^{-6}	10^{-5}	10^{-6}	10^{-5}	10^{-6}
$\Gamma_t = 0, m_q$						
$\hat{\sigma}^{\text{1-loop}}$	-3.2657(4)	-3.2666(6)	39.71(1)	39.70(1)	50.22(2)	50.22(2)
δ , %	-172.64(1)	-172.66(1)	-14.95(2)	-14.96(3)	-0.99(3)	-1.00(4)
$\hat{\sigma}^{\overline{\text{MS}}}$	6.5587(4)	6.5586(6)	45.29(1)	45.29(1)	50.53(2)	50.52(2)
$\delta^{\overline{\text{MS}}}$, %	45.88(1)	45.88(1)	-2.98(2)	-2.99(3)	-0.38(3)	-0.39(4)
$\Gamma_t = 0, m_q/10$						
$\hat{\sigma}^{\overline{\text{MS}}}$	6.5564(7)	6.5553(9)	45.28(2)	45.28(2)	50.51(3)	50.53(3)
$\delta^{\overline{\text{MS}}}$, %	45.91(2)	45.88(2)	-3.01(4)	-3.02(4)	-0.42(5)	-0.39(6)
$\Gamma_t \neq 0, m_q$						
$\hat{\sigma}^{\text{1-loop}}$	-3.1526(4)	-3.1532(5)	39.99(1)	39.99(1)	50.52(1)	50.51(2)
δ , %	-170.12(1)	-170.14(1)	-14.35(2)	-14.34(3)	-0.40(3)	-0.41(3)

Table 17. The same as in Table 15 but for $\text{pid} = 28$. Process $b + \bar{d} \rightarrow \bar{u} + t$ ($\sigma^{\text{Born}} = 4.495790646(3)$ pb)

Cross section, correction	$\Gamma_t/10^0$	$\Gamma_t/10^2$	$\Gamma_t/10^4$	$\Gamma_t = 0$
$\hat{\sigma}^{\text{1-loop}}$, pb	-3.1526(4)	-3.2644(4)	-3.2661(5)	-3.2657(4)
δ , %	-170.12(1)	-172.61(1)	-172.65(1)	-172.64(1)

proof shown in Sec.2 for the s channel). So, it should be considered as only a formal, numerical illustration of convergence.

Table 16 is the counterpart for QCD of the six Tables 18–22 of [12].

From Tables 16, 17 the same conclusions may be drawn as from Tables 14, 15. We will not repeat them here.

4. CONCLUSIONS AND OUTLOOK

In two papers, this one and [12], we have described the implementation into the SANC framework of the complete one-loop QCD and EW calculations, including hard bremsstrahlung contributions, for the processes of top-quark decays and of s - and t -channel production, the latter two at the partonic level. Within the SANC framework, we have created the standard FORM and FORTRAN modules, see, [23], compiled into a package `sanc_cc_v1.40` which may be downloaded from the SANC project homepages [24].

The essentially new aspect of these two papers is the study of regularization of the top quark–photon and quark–gluon infrared divergences with the aid of the complex mass of the top quark. A comparison of these NLO corrections computed within this approach with those computed by the conventional method showed a difference which is not negligible,

though not exceeding $\sim 1\%$ for both types of corrections and for three considered processes. Although, the introduction of the nonzero top width within the fixed width scheme violates gauge-invariance, it is numerically not so important being of the order $\mathcal{O}(\Gamma_t/m_t)$; it restores in the limit $\Gamma_t \rightarrow 0$.

The emphasis of these papers is to be assured of the correctness of our results. We observe the independence of the form factors on gauge parameters, checked the stability of the result against variation of the soft–hard separation parameter $\bar{\omega}$ and the independence of the $\overline{\text{MS}}$ subtracted quantities off the initial quark masses which is crucial for calculations at the hadronic level.

As has become SANC standard, we have compared our numerical results with other independent calculations wherever possible. For the decay channels it was done in our previous papers (both EW [25] and QCD [26]), showing good agreement. As usual, the Born level and the hard gluon contributions of all three channels were checked against the CompHEP package. We found very good agreement for both $\Gamma_t = 0 (\neq 0)$ options.

As far as the comparison of EWRC for the production processes is concerned, it was described in our previous paper [12] and we found no suitable results in the literature on QCD corrections at the partonic level.

As a first step toward comparison of QCD calculations at the hadronic level we performed a triple comparison of the LO total cross sections of s - and t -channel single top-quark production computed by SANC/CompHEP/MCFM with the same set of PDF. We found a satisfactory agreement between SANC and CompHEP numbers. The comprehensive comparison of the results at the hadronic level is the subject of ongoing work and a further publication.

All the calculations were done using a combination of analytic and Monte Carlo integration methods which will make it easy to impose experimental cuts in future calculations for pp collisions at the hadronic level. The results presented in these two papers lay a solid base for future extensions of calculations for the single top-production channels at the LHC with subsequent decay in the cascade (factorized) approximation (see, e.g., [27]) which simultaneously take account of NLO EW and QCD corrections.

Acknowledgements. This work is partly supported by Russian Foundation for Basic Research, grant No. 10-02-01030. WvS is indebted to the directorate of the Dzhelapov Laboratory of Nuclear Problems, JINR, Dubna, for the hospitality extended to him during April 2011.

REFERENCES

1. *Bernreuther W.* // J. Phys. G. 2008. V. 35. P. 083001.
2. *Abazov V. M. et al.* // Phys. Rev. Lett. 2007. V. 98. P. 181802.
3. *Abazov V. M. et al.* // Phys. Rev. Lett. 2009. V. 103. P. 092001.
4. *Aaltonen T. et al.* // Phys. Rev. Lett. 2008. V. 101. P. 252001.
5. *Aaltonen T. et al.* // Phys. Rev. Lett. 2009. V. 103. P. 092002.
6. *Chatrchyan S. et al.* Preprint arXiv: 1106.3052 [hep-ex].
7. *Harris B. W. et al.* // Phys. Rev. D. 2002. V. 66. P. 054024.
8. *Campbell John M. et al.* // Phys. Rev. Lett. 2009. V. 102. P. 182003.
9. *Sullivan Zack* // Phys. Rev. D. 2004. V. 70. P. 114012.

10. *Frixione St. et al.* // JHEP. 2006. V. 03. P. 092.
11. *Boos E. E. et al.* // Phys. Atom. Nucl. 2006. V. 69. P. 1317–1329.
12. *Bardin D. et al.* // Eur. Phys. J. C. 2011. V. 71. P. 1533.
13. *Denner Ansgar et al.* // Nucl. Phys. B. 1999. V. 560. P. 33–65.
14. *Kidonakis N.* // Phys. Rev. D. 2011. V. 83. P. 091503.
15. *Denner Ansgar, Dittmaier S.* // Nucl. Phys. Proc. Suppl. 2006. V. 160. P. 22–26.
16. *Actis St. et al.* // Phys. Lett. B. 2008. V. 669. P. 62–68.
17. *Andonov A. et al.* // Comput. Phys. Commun. 2006. V. 174. P. 481–517.
18. *Bardin D. et al.* // Eur. Phys. J. C. 2007. V. 52. P. 83–92.
19. *Passarino G., Veltman M. J. G.* // Nucl. Phys. B. 1979. V. 160. P. 151.
20. <http://comphep.sinp.msu.ru/>. v.4.4.3. 2004.
21. <http://comphep.sinp.msu.ru/>. v.4.5.1. 2009.
22. *Kidonakis N.* Preprint arXiv:1109.3231 [hep-ph].
23. *Andonov A. et al.* // Comp. Phys. Commun. 2010. V. 181. P. 305–312.
24. Dubna — <http://sanc.jinr.ru>, CERN — <http://pcphsanc.cern.ch>
25. *Arbuzov A. et al.* // Eur. Phys. J. C. 2007. V. 51. P. 585–591.
26. *Andonov A. et al.* // Part. Nucl., Lett. 2007. V. 4. P. 451–460.
27. *Bardin D. et al.* // Part. Nucl., Lett. 2010. V. 7. P. 72–79.

Received on November 2, 2011.